

MIT Open Access Articles

Manifold#based respiratory phase estimation enables motion and distortion correction of free#breathing cardiac diffusion tensor MRI

The MIT Faculty has made this article openly available. **Please share** how this access benefits you. Your story matters.

Citation: Coll#Font, Jaume, Chen, Shi, Eder, Robert, Fang, Yiling, Han, Qiao Joyce et al. 2021. "Manifold#based respiratory phase estimation enables motion and distortion correction of free#breathing cardiac diffusion tensor MRI." Magnetic Resonance in Medicine, 87 (1).

As Published: <http://dx.doi.org/10.1002/mrm.28972>

Publisher: Wiley

Persistent URL: <https://hdl.handle.net/1721.1/140429>

Version: Author's final manuscript: final author's manuscript post peer review, without publisher's formatting or copy editing

Terms of Use: Article is made available in accordance with the publisher's policy and may be subject to US copyright law. Please refer to the publisher's site for terms of use.



Title: Manifold-based Respiratory Phase Estimation Enables Motion and Distortion Correction of Free-Breathing Cardiac Diffusion Tensor MRI

Author Names: Jaume Coll-Font^{1,2,3}, Shi Chen¹, Robert Eder¹, Yiling Fang^{1,4}, Qiao Joyce Han^{1,3}, Maaïke van den Boomen^{1,2,3,5}, David E. Sosnovik^{1,2,3}, Choukri Mekkaoui^{1,3}, and Christopher T. Nguyen^{1,2,3}

Author Affiliations

1. Cardiovascular Research Center, Massachusetts General Hospital, Boston (MA), USA
2. Athinoula A. Martinos Center for Biomedical Imaging, Massachusetts General Hospital, Boston (MA), USA
3. Harvard Medical School, Boston (MA), USA
4. Institute of Medical Engineering and Science, Massachusetts Institute of Technology, Cambridge, (MA), USA
5. Department of Radiology, University Medical Center Groningen, Groningen, Netherlands

Corresponding Author Info: Christopher T. Nguyen, 149 13th St, 4th floor, 02129, Charlestown (MA), USA. 617-643-7838, Nguyen, Christopher.Nguyen@mgh.harvard.edu

Grant Support: Funding from the National Institutes of Health: R01 HL35242, R01 HL151704, R01 HL141563, and R01 HL131635. Additional support from the Hassenfeld Scholar Award and MGH Corrigan SPARK Award.

Running Title: Motion and Distortion Correction of Free-Breathing Cardiac Diffusion Tensor MRI

Total word count: 4893

This is the author manuscript accepted for publication and has undergone full peer review but has not been through the copyediting, typesetting, pagination and proofreading process, which may lead to differences between this version and the [Version of Record](#). Please cite this article as [doi: 10.1002/MRM.28972](https://doi.org/10.1002/MRM.28972)

This article is protected by copyright. All rights reserved

DR. JAUME COLL-FONT (Orcid ID : 0000-0001-9341-6838)

DR. CHRISTOPHER T NGUYEN (Orcid ID : 0000-0003-1475-2329)

Article type : Research Article

Manifold-based Respiratory Phase Estimation Enables Motion and Distortion Correction of Free-Breathing Cardiac Diffusion Tensor MRI

Jaume Coll-Font^{1,2,3}, Shi Chen¹, Robert Eder¹, Yiling Fang^{1,4}, Qiao Joyce Han^{1,3},
Maaïke van den Boomen^{1,2,3,5}, David E. Sosnovik^{1,2,3}, Choukri Mekkaoui^{1,3}, and
Christopher T. Nguyen^{1,2,3}

¹Cardiovascular Research Center, Massachusetts General Hospital, Boston (MA), USA.

²Athinoula A. Martinos Center for Biomedical Imaging, Massachusetts General Hospital, Boston (MA), USA.

³Harvard Medical School, Boston (MA), USA.

⁴Institute of Medical Engineering and Science, Massachusetts Institute of Technology, Cambridge, (MA), USA.

⁵Department of Radiology, University Medical Center Groningen, Groningen, Netherlands.

ABSTRACT

PURPOSE

For in-vivo cardiac diffusion-tensor imaging (DTI), breathing motion and B_0 field inhomogeneities produce misalignment and geometric distortion in diffusion weighted (DW) images acquired with conventional single shot echo planar imaging (EPI). We propose using a dimensionality reduction method to retrospectively estimate the respiratory phase of DW images and facilitate both distortion correction (DisCo) and motion compensation (MoCo).

METHODS

Free-breathing ECG-triggered whole left-ventricular (LV) cardiac DTI using a second order motion compensated spin echo EPI sequence and alternating directionality of phase encoding blips was performed on eleven healthy volunteers. The respiratory phase of each DW image was estimated after projecting the DW images into a 2D space with Laplacian Eigenmaps. DisCo and MoCo was applied to the respiratory sorted DW images. The results were compared against conventional breath-held HASTE. Cardiac DTI parameters including fractional anisotropy (FA), mean diffusivity (MD), and helix angle transmural (HAT) were compared with and without DisCo.

RESULTS

The LV geometries after DisCo and MoCo resulted in significantly improved alignment of DW images with HASTE reference. DisCo reduced the distance between the LV contours by $13.2 \pm 19.2\%$ $p < 0.05$ (2.0 ± 0.4 for DisCo and 2.4 ± 0.5 mm for uncorrected). DisCo DTI parameter maps yielded no significant differences (MD: $1.55 \pm 0.13 \times 10^{-3} \text{mm}^2/\text{s}$ and $1.53 \pm 0.13 \times 10^{-3} \text{mm}^2/\text{s}$, $p = 0.09$; FA: 0.375 ± 0.041 and 0.379 ± 0.045 , $p = 0.11$; HAT: 1.00 ± 0.10 $^\circ/\%$ and 0.99 ± 0.12 $^\circ/\%$, $p = 0.44$), although the orientation of individual tensors differed.

CONCLUSION

Retrospective respiratory phase estimation with LE-based DisCo and MoCo in free-breathing cardiac DTI resulting in significantly reduced geometric distortion and improved alignment within and across slices.

Keywords:

Diffusion Tensor Imaging; Free-breathing; Distortion correction; Motion compensation; Cardiac MRI; Laplacian Eigenmaps.

INTRODUCTION

Cardiac diffusion-tensor imaging (DTI) is a promising imaging technique to evaluate the microstructure of the heart. Diffusion tensors represent the diffusivity of the tissue and reflect tissue characteristics of the myocardial microstructure (1). The technique has been shown to provide information about myocardial structural remodeling in pathologies such as hypertrophic cardiomyopathy, dilated cardiomyopathy, and myocardial infarction (2–5).

The recent introduction of second order motion compensated (M2) diffusion gradient encoding enabled acquisition of a diffusion weighted (DW) image per heartbeat, thus minimizing both cardiac and respiratory motion-induced signal loss, which consequently allows free-breathing acquisition (6–11). Complementary to M2 encoding, the implementation of two-dimensional spatial selective radiofrequency (2DRF) zoomed echo planar imaging (EPI) provided a reduced temporal footprint (~20ms) and further improved signal-to-noise (SNR) and spatial resolution(12). However, large thoracic B_0 field inhomogeneities still persist in introducing geometric distortion to the images acquired with EPI readout. This distortion can be problematic for applications that require accurate geometry such as spatial correlation studies with alternative mapping techniques –*e.g.* T1, T2 mapping— or to build finite element models of the heart.

Despite of the extensive work in DW imaging on distortion, most methods assume minimal motion among the acquired images and cannot account for B_0 field dependance on respiration(13, 14). In consequence, performing distortion correction (DisCo) remains being a challenge for free-breathing cardiac DTI. Here, we introduce a

novel technique to estimate the respiratory motion by the retrospective application of DisCo and motion compensation (MoCo), using a manifold-based technique (Laplacian Eigenmaps) to project free breathing DW images onto a lower-dimensional representation. The projections are then used to align DW images with matching respiratory phase and facilitate the retrospective DisCo and MoCo of free-breathing cardiac DTI.

THEORY

Respiration Phase Estimation

The most prominent mode of variation in DW images acquired during ECG-triggered free-breathing is the respiratory phasic movement of the heart. Since this motion is smooth and repetitive throughout the respiratory cycle, the DW images, represented as points in a high-dimensional space of size equal to the number of voxels in the image, form a manifold of dimension 1 and the relative position of each image within this 1D manifold corresponds to its respiratory phase. Similarly, the contrast differences introduced by the DW encoding add another mode of variation to the images and, consequently, another dimension to the manifold. In order to take advantage of the two dominant dimensions of the manifold, it must be projected into a lower dimensional space for interpretation. This step is achieved with a manifold embedding technique such as Laplacian Eigenmaps (LE) (15–17). As shown in Figure 1, LE generates a low dimensional representation such that each image in the original dataset is mapped onto a point in 2D space. The learned mapping ensures that the manifold structure is preserved by preserving local distances between the N images in the original dataset $\{x_i\}$ (15). This optimization procedure is achieved by first computing a similarity matrix

$W \in \mathbb{R}^{N \times N}$ between every pair of DW images (x_i, x_j) , $W_{i,j} = e^{-\frac{\|x_i - x_j\|^2}{\sigma}}$ for some $\sigma > 0$, and then solving the generalized eigenvalue problem ($Lf = \lambda Df$) over the matrices $D \in \mathbb{R}^{N \times N}$, a diagonal matrix formed by $D_{i,i} = \sum_j W_{j,i}$, and the graph Laplacian matrix $L = D - W$. For more details about the derivation of LE, we refer the reader to Belkin and Niyogi (15). The resulting eigenvectors $\{f_k\}_{k=0}^{K-1}$ form the low dimensional

representation of the DW images. In other words, the n^{th} entry in the eigenvector f_k corresponds to the k^{th} dimension of the image x_n in the low dimensional representation.

$$x_n \rightarrow (f_1(n), f_2(n))$$

Since the objective of LE is to preserve the distance between points in the low dimensional representation, the metric used to compute the affinity matrix W is essential to the estimation of this representation. Standard implementations of LE use the Euclidean norm $\|x_i - x_j\|^2$ to measure their distance. Unfortunately, this metric can be sensitive to non-Gaussian sources of noise such as aliasing artifacts. To overcome this limitation, we used mutual information instead, which has been shown to be more robust than mean-squared distance in the registration of images with distinct contrasts(18). Hence, the affinity matrix was modified to:

$$W_{i,j} = e^{-\frac{1-MI(x_i, x_j)}{\sigma}},$$

Where the $MI(x_i, x_j)$ corresponds to the mutual information metric between DW images (x_i, x_j) and was computed using 256 bins and $\sigma = \max(1 - MI(x_i, x_j))$. The low-dimensional representation of the DW images obtained using this technique, illustrated in Figure 1, results in two elongated point-clouds of DW images. Each cloud corresponds to one b-value ($b=50$ and 500 s/mm^2) and their elongated direction to the changes along respiratory phase. Points at opposing edges of the same point-cloud correspond to DW images with the same b-value but at opposite ends of the respiratory cycle –i.e. expiration or inspiration. Consequently, the respiratory phase of the DW images can be estimated as their position along the elongated direction within each point-cloud. This position is then computed by projecting all images into the first component in a principal component analysis (PCA) decomposition. The respiratory phase is then estimated after normalizing the projected points between -1 and 1 and ensuring that the ends of the estimated respiratory cycle correspond to maximum inhale (-1) and maximum exhale (+1).

Distortion Correction

Geometric distortion due to B_0 field inhomogeneities is characterized by local compression and elongation of the tissue in the reconstructed images (19–21). Whether the distortion effect is compression or elongation depends on the local field inhomogeneities and the direction of the phase readout direction in the EPI acquisition – *e.g.* anterior-posterior and posterior-anterior. This characteristic is typically used in registration-based DisCo techniques, which consist of acquiring two images with opposite phase encoding direction and co-registering them to estimate the B_0 field inhomogeneities (21–24). These techniques assume that the B_0 field inhomogeneities are the same for both images and, under the further assumption that these inhomogeneities remain stable throughout the scan, the estimated field can be used to correct for distortion in any subsequently acquired image (22). Unfortunately, these assumptions are not valid for free breathing cardiac DT-MR due to respiratory motion (25). Breathing introduces respiratory dependent changes to the B_0 field impeding the use of standard registration-based DisCo (13, 14, 26). Thus, in order to apply any registration-based DisCo technique to free-breathing cardiac DTI, it is necessary to first match DW images with similar respiratory phase to ensure that the B_0 field estimation is performed on pairs of images with similar B_0 fields.

Free-breathing DisCo begins by sorting the DW images into 3D stacks composed of the 2D images over time, sorted along respiratory phase. This procedure results in one ‘2D-resp’ stack per b-value, slice, and phase encoding direction. Afterwards, the 2D-resp stacks acquired with opposite phase encodings and b-value $b=50\text{s/mm}^2$ are paired and introduced into a standard registration-based DisCo implementation – *e.g.* TOPUP(22)— to estimate the B_0 field for the entire set of $b=50\text{s/mm}^2$ images in the stack. Even though not all DW images in each 2D-resp stack will be perfectly aligned in respiratory phase with its counterpart in the opposite phase encoding, the 3D smoothing (here 2D+resp phase) within the B_0 field estimation procedure compensates for these misalignments and provides a continuously varying B_0 field over respiratory cycle. After the 2D-resp B_0 field is estimated per each slice, these are used to correct for geometric distortion in the rest DW 2D-resp stacks for all b-values and slices.

Motion Compensation

Motion compensation is a necessary step in free-breathing cardiac DTI due to the displacement of the heart within the FOV in the images. However, registration of DW images is challenging due to the differences in contrast across b-values as well as the lack of a common registration reference across slices. To overcome this limitation, the proposed method uses the respiration phases, estimated with LE, to independently register the groups of images with the same b-value and slice position to a predetermined respiratory phase reference. Even though DW images in different groups are registered to a different reference image, the common respiratory phase of the references ensures that the DW images are aligned regardless of their b-value or slice position. In practice, the common respiratory phase was chosen to be the end-expiration phase since it was empirically observed to be more stable across slices.

In order to minimize computational demands, we take advantage of a binning approach previously used in conjunction with a low-rank decomposition method to perform registration (11). In the current work, each b-value and slice group of DW images is binned into 5 bins by dividing their respiratory phases into equally spaced bins between -1 and 1. Afterwards, the centroid of each bin is computed as the median of all the images in it and registered to the end-expiration reference. The learned transformations are finally applied to all DW images within each bin to align the entire set of images. The overall MoCo algorithm is summarized in the following steps:

- 1- For every slice and b-value:
 - a. Group all DW images into sets with the same b-value and slice position.
 - b. Bin all DW images in each group into 5 respiratory bins.
 - c. Register the centroid of each bin to the end-expiration reference.
 - d. Apply the learned registration transform to all images within each bin.

METHODS

Eleven healthy volunteers (mean age 43 years, 5 female) were recruited under the appropriate approval from the institutional review board of the Massachusetts General Hospital. Cardiac MRI was performed on a 3T clinical MRI system

(MAGNETOM Prisma, Siemens Healthineers, Erlangen, Germany), equipped with an 80mT/m gradient system and a standard 32-channel antero-posterior surface coil. The subjects were instructed to breathe freely during the acquisition. The DTI-MR acquisition was done with M2 2DRF zoomed EPI with the following parameters (30 directions at $b = 50 \text{ s/mm}^2$, 30 directions x 2 averages at $b = 500 \text{ s/mm}^2$, $2.5 \times 2.5 \times 8 \text{ mm}^3$ without slice gap, matrix size 150×44 , pixel bandwidth (BW) 2380 Hz/pixel , $1/3$ reduced FOV, $\text{FOV} = 375 \text{ mm}$, Partial Fourier = $6/8$, $\text{TE} = 79 \text{ ms}$, TR determined by the ECG trigger). The images were acquired during systole, with short axis view and enough slices to cover the entire LV (12 to 16 depending on the subject). The phase encoding orientation was selected to be along the anterior-posterior direction although it was modified to minimize the aliasing artifacts on the LV. Each DTI scan was repeated twice, each time reversing the phase encoding direction by 180° to generate acquisitions with opposite phase encoding. The average time to acquire all the DW images for one phase encoding direction was $22.6 \pm 3.9 \text{ min}$, resulting in a total of $45.3 \pm 7.7 \text{ min}$ for the entire DisCo protocol. The scanning protocol also included the acquisition of a T_2 Half-Fourier Single Shot Turbo Spin Echo (T_2 -HASTE) under breath-hold to serve as a distortion-free reference against which the DisCo geometries were compared ($\text{TE} = 36 \text{ ms}$, $\text{TR} = \text{ECG trigger}$, (BW) 1860 Hz/pixel , matrix size 128×96 and voxel size $1.125 \times 1.125 \text{ mm}$).

A second group of four volunteers (mean age 39.5, 3 female) were recruited, to evaluate the performance of the LE-based registration, also under appropriate approval from the institutional review board of the Massachusetts General Hospital. These volunteers were imaged with a modification of the M2 2DRF zoomed EPI DTI-MR sequence that includes a pencil navigator echo, manually placed on top of the liver dome to track respiratory phase. The acquisition parameters were set to match those of the previous subjects except for the order of slice acquisition, which was sequential per each slice, and only one phase encoding direction was acquired.

Data Processing

The acquired data was first cropped to ensure a field-of-view centered around the heart. Afterwards, the images were processed following the pipeline described in the

theoretical section and illustrated in the flow diagram in Figure 1. In short, the DW images for each phase encoding and slice were sorted according to their respiratory phase into 2D-resp stacks and TOPUP was used to estimate the B_0 field inhomogeneity on each pair of stacks acquired with DW $b=50 \text{ s/mm}^2$ and opposite phase encoding. The estimated fields were then used to correct for distortion in the rest of 2D-resp stacks. Before registration, all images were resampled to isotropic resolution of 128×128 pixels. Registration was then applied to the 5 respiratory bin centroids of each b -value and slice group. These were registered to the bin at end-expiration as reference and with affine registration implemented in ELASTIX(27). The DW images were then transformed using the registration parameters learned for their corresponding respiratory bin. Finally, the DTI model was fitted using weighted least squares implementation in DIPY(28) and the fractional anisotropy (FA), mean diffusivity (MD) and helix angle (HA) were computed. Helix angle transmurality (HAT) –*i.e.* the change in HA per percent of transmural depth— was computed within 100 lines per slice by fitting a linear model to all the points in each section using linear regression with in-house implementation.

To estimate the respiratory phase from the navigator echoes, the navigator images were segmented semi-automatically to extract the position of the top of the liver for each acquisition. Afterwards, these were normalized between -1 and 1 (end-expiration and end-inspiration respectively). The resulting ‘navigator’ respiratory phases were then compared to those obtained with LE by computing the Pearson correlation coefficient between traces of respiratory phase in each subject and slice.

Image processing was performed with a python pipeline interfacing with TOPUP and ELASTIX using SimpleITK(29, 30). Left ventricle (LV) masks were generated manually by JCF and SC with Seg3D(31). The masks of the distortion-free reference were generated using the T_2 -HASTE images and those for the DW images were generated using the reference used for registration as well as the scalar DTI parameter maps (MD, FA and HA). The similarity between the T_2 -HASTE masks and those generated with the DW images was assessed with the average distance between their contours. In order to compensate for differences in position of the heart during breath-hold and end-expiration, the LV masks of the T_2 -HASTE and the DTI results were

registered using 3D rigid registration in ELASTIX before computing the difference. All statistical tests were performed using SCIPY(32) with non-parametric Wilcoxon tests(33) and the differences were considered significant for $p < 0.05$.

RESULTS

Figure 2 illustrates the low dimensional representation of the DW images for an example subject for whom navigator echoes were acquired. The LE representation formed two elongated clusters, one per b-value, where the long axis dimension corresponded to the respiratory phases obtained with the navigator echoes. The second axis, particularly for the $b=500\text{s/mm}^2$ cluster, is mostly dominated by differences in contrast due to different gradient orientations. The respiratory phases estimated with both LE and the navigator echoes presented good agreement over time and, sorting the DW images according to either respiratory phase resulted in similarly smooth transitions of the heart between end-expiration to end-inspiration. Numerically, the person correlation coefficient between LE and navigator respiratory phases, averaged over 4 subjects, was 0.72 ± 0.14 further indicating good agreement between the two approaches.

The respiratory phases estimated with LE allowed to sort the $b=50\text{s/mm}^2$ images into 2D-resp stacks and to compute the B_0 field inhomogeneities across different respiratory phases. As seen in Figure 3, the resulting B_0 field varied smoothly over the two spatial dimensions as well as over respiratory phase. Figure 4 compares the raw images before and after applying DisCo to the corresponding T_2 -HASTE reference for a representative subject. Before DisCo, the images presented either compression or elongation (indicated as 'Cp.' and 'El.') of the LV free wall along the phase encoding direction. After DisCo, the LV was rounder and more similar to that of the T_2 -HASTE reference. This shape improvement is further illustrated in Figure 5 with the LV mask contours for 5 representative subjects selected based on the distance between masks generated with their DW and T_2 -HASTE images. Specifically, we chose the two subjects with most reduction in distance after applying DisCo, a subject with median reduction, and the two with the least reduction in distance. The contours of the LV masks

generated using the DisCo images (red) matched better with the contour of the LV in the T₂-HASTE than those obtained from the uncorrected images (yellow). Even for the worst cases (last two columns), DisCo did not introduce major artifacts although it could not compensate for their large distortion. The distances between the T₂-HASTE mask contours and those generated from the DW images are reported in the scatter plot of Figure 5. This plot compares the LV mask distances of the uncorrected images (vertical axis) and of the DisCo images (horizontal axis). Hence, points above the identity line (dashed line) resulted in a reduction in distance between LV masks, points on the line showed no difference and points below the line had an increase in distance. Most cases resulted in reduced distance after DisCo –15 cases with >10% improvement—, some cases showed small difference –6 cases within 10% variation— and only a few cases presented an increase of error –3 cases had > 10% increase in distance. On average the LV mask distance was 2.0+/-0.4 mm for the DisCo images and 2.4+/-0.5 mm for the uncorrected ones. The average reduction in distance was of -0.4+/-0.5 mm (p<0.05), which corresponds to 13.2+/-19.2% reduction over the uncorrected LV mask distance.

LE-based registration was successful in aligning the series of DW images of each subject. Figure 6 shows a line of voxels plotted over respiratory phase for 4 representative subjects. Before MoCo, the heart was smoothly displaced downwards between the end-expiration and end-inspiration. After applying MoCo, the respiratory motion was suppressed, and all the time instances were aligned with each other and remained at the end-expiration position. Moreover, the end-expiration reference provided consistent registration across slices. As shown in Figure 7, the masks generated with the MoCo masks (red contours) resulted in reduced through-slice changes when compared to the uncorrected (yellow contours). The corrected masks were continuous along the long axis view and aligned well with the T₂-HASTE reference acquired during breath-hold.

The DTI fits resulted in no differences between the scalar parameter maps (MD, FA and HAT) obtained with DisCo and uncorrected DW images. Figure 8 shows the DTI parameter distribution for all subjects. The average values within the LV mask for DisCo and raw images were, respectively, 1.55+/-0.13 x10⁻³mm²/s and 1.53+/-0.13 x10⁻³mm²/s (p=0.09) for MD; 0.375+/-0.041 and 0.379+/-0.045 (p=0.11) for FA; 1.00+/-0.10 °/% and

0.99 \pm 0.12 % (p=0.44) for HAT. Similarly, the compressed and elongated parameter maps showed no significant differences between MD, FA and HAT (Supplementary material Table S1). The histogram of the parameters MD, FA and HA were similar for all combinations of compressed/elongated and corrected/uncorrected, except for some slight deviation in the HA values in some subjects (Supplementary Figure S1 and S2). The parameter maps, illustrated in Figure 9, also presented similar values between DisCo and uncorrected results besides a change of shape of the LV. However, the maps obtained with elongated phase encoding resulted in loss of transmural differentiation and an HA close to 0 in the most elongated areas. DisCo was not capable of correcting for these errors, suggesting that it is preferable to acquire the images with the phase encoding direction that results in compression. Despite the similarity of parameters between DisCo and uncorrected results, the geometric distortion introduced differences in the orientation of the diffusion tensors due to the change of shape of the LV, due to the changes in its geometry (Figure 10). As a result, the tensors in the LV presented better agreement in orientation and geometry alignment between the compressed and elongated datasets after performing DisCo. Specifically, the inner product between primary eigenvectors, averaged across all voxels within the LV mask of both compressed and elongated geometries, increased to 0.61 \pm 0.09, compared to 0.53 \pm 0.09 before DisCo (p<0.05). Similarly, the overlap between compressed and elongated LV geometry increased to 0.80 \pm 0.07 from 0.7 \pm 0.07 (p<0.05).

DISCUSSION

LE can be used to identify the respiratory phase of DW images in free-breathing cardiac DTI, facilitating both DisCo and MoCo. In healthy volunteers, LE-based DisCo resulted in 13.2% closer distance between the LV contours generated using the distortion-free T₂-HASTE images compared to those generated with distorted DW images. The reduction in distortion resulted in changes in the orientation of the DTI models, although it did not affect the scalar parameters.

Mitigating the effects of distortion is typically achieved with the reduction the number of k-space lines acquired during the EPI readout, at the cost of reduced FOV or

image resolution(19). On this regard, 2DRF zoomed EPI provided considerable improvement by allowing the reduction of the FOV without incurring in large aliasing artifacts(12). However, distortion is still present in the zoomed DW images and requires correction. A previous approach that considered motion in DW imaging of children used a dual-echo sequence to acquire two readouts in opposite phase encoding directions for each DW image(34–36). The short time between the dual-echo readouts ($\sim 30\text{ms}$) allowed the assumption that there is no motion between the two images, and standard DisCo techniques could be applied. However, this technique could not be used in cardiac imaging due to the short T_2 decay of the myocardium compared to the long TE for the second readout, which is on the order of $\sim 100\text{ms}$. Alternative DisCo approaches that consider motion made numerical approximations to estimate the change in B_0 field inhomogeneities due to motion, or implemented a deep-learning model to register the DW images to a distortion-free reference(25, 37). Unfortunately, the assumptions used to model the B_0 field fail for large changes observed during breathing observed for the heart and approaches that use registration of the DW images to a distortion free reference are known to be prone to errors(38).

To our knowledge, there are only two methods that have been proposed to perform distortion correction in cardiac DTI. Tunnicliffe *et al.* first proposed using registration-based methods to correct for distortion in breath held scans(39). More recently, van Gorkum *et al.* introduced a distortion correction method that takes advantage of the multi-coil acquisition to correct for the off-resonance effects during reconstruction(40). Their method requires availability of the raw k-space data to perform the multi-coil image reconstruction as well as an estimation of the B_0 field map to introduce the off-resonance corrections. In consequence, this method requires using prospective navigator to account for breathing motion and has the inherent assumption that the B_0 field does not change within the navigator gating window. Our method relaxes this assumption by allowing the B_0 field to change smoothly over the breathing cycle.

Interestingly, Gorkum *et al.* report better distortion correction when acquiring elongated direction, compared to compressed. Even though our results show no significant difference between elongated and compressed parameter maps nor contour

distance to the HASTE images, we have subjectively observed some deterioration of the HA maps for elongated areas. This discrepancy is worth exploring although there are several causes that could have created it. First, the DW imaging protocols used in both experiments differ in the sampling approaches of Q-space. Moreover, Gorkum *et al.* used gated navigators and slice tracking(41) to avoid breathing motion, while in the present experiments, the volunteers could breathe freely without any instructions or guidance. Second, the two distortion correction methods are different in how they estimate the B_0 field maps and then apply the distortion correction. The proposed method applies the distortion correction through spatial transformations of the images and cannot correct for intensity changes. On this regard, the method proposed by van Gorkum *et al.* could potentially correct for those during image reconstruction. In the future, it would be interesting compare both methods and to assess whether the B_0 field maps estimated with the proposed approach could be used as an input to the multi-coil reconstruction method proposed by van Gorkum *et al.*.

Manifold embedding was previously used to estimate respiratory motion in the context of cardiac MRI(16, 42). These methods used standard LE to bin the raw k-space data and generate MoCo for CINE reconstructions. Moreover, a recent manifold embedding approach was introduced to jointly estimate the low-dimensional representations of raw k-space data acquired with slightly different views(43). Even though the data characteristics are different from the application presented here – continuously acquired raw k-space data versus ECG-gated DW images— this joint manifold embedding method could be used to jointly learn the LE representation of all slices and phase encodings.

Respiratory motion for in vivo cardiac DTI is typically addressed through breath-hold acquisition. However, breath-holds extend scan time and can be challenging for patients with dyspnea(44). An alternative approach is to prospectively include respiratory binning, obtained with image navigators or external sensors(45). The disadvantages of these methods are the need of manual intervention during the scan to set a navigator line or calibrating the measurement system and, more importantly, can increase the acquisition time due to the rejected bins. In contrast, retrospective

approaches –such as the one presented here— do not present these limitations but require retrospective registration, which might be challenging given the contrast differences in DW imaging. Typical registration methods use metrics that offer robustness to contrast differences (*e.g.* Mutual information)(18), minimize the variance or discrepancy of the registered volumes over time(46), use image segmentation as reference(47), or attempt to model the motion or the diffusion signal to further regularize the registration(48–50). These methods often require intense computational demands nor facilitate through-slice alignment. LE-based MoCo overcomes these challenges by only registering respiratory bin centroids and separating DW images by b-value and slice during registration. This binning approach was recently introduced in conjunction with a method that computed a low-rank tensor decomposition of the DW images to eliminate contrast differences before registration(11). In that work, k-means was used to perform the image binning to facilitate registration and demonstrated reduced computational demands as well as improved registration accuracy. In this context, the respiratory phases estimated with LE provide a continuous ordering of the DW images that is not affected by contrast differences and can provide an alternative binning approach to k-means. These respiratory phases could also be estimated with other methods such as the use of pneumatic belts or navigator echoes, which have the potential of being more accurate. However, these require external hardware or modifications to the acquisition sequences that are not always readily available, as well as manual intervention during the scan to place the belts or the navigator beam. On the other hand, retrospectively estimating the respiratory phases through registration techniques would incur into increased computational costs which undermine the computational savings of solely registering the bin centroids.

Limitations

A limitation of the present study is the extended scan time needed to acquire the two sets of DW images with opposite phase encoding. This scan time, however, can be greatly reduced since the B_0 field inhomogeneities are estimated with solely the DW images at $b=50 \text{ s/mm}^2$. In future work, we will limit the DisCo protocol to two sets of DW

images at $b=50 \text{ s/mm}^2$ with opposite phase encodings and a set of images at $b=500 \text{ s/mm}^2$ acquired along a single phase encoding. Thus, the resulting DisCo protocol will require the addition of only 30 volumes, which would extend the acquisition time by approximately 6 min with respect to a non-DisCo acquisition.

A conclusion derived from this work is that geometric distortion does not affect the DTI parameter estimates but distorts the geometry of the maps. The latter effect is important when patients are imaged with multiple modalities and MR contrasts to localize injured tissue. For example, patients with myocardial infarction could be imaged with cardiac DTI and late-gadolinium enhancement and would consequently benefit from the geometric alignment of both modalities after applying DisCo. Future work should include the enrolment of patients and assess co-localization of injuries imaged with cardiac DTI as well as T_1/T_2 mapping or late-gadolinium enhancement.

Finally, there are two key assumptions with respect to the motion of the heart due to breathing that must be considered. First, the current registration approach is limited to two dimensions. In consequence, through plane motion cannot be corrected and introduces error. Second, the estimation of respiratory phases assumes that the breathing cycle is approximately constant over the entire acquisition and does not contain isolated deep breaths or respiratory drift (51). In the presence of large drifts of the respiratory cycle, the 2D-resp stacks used to estimate the B_0 field inhomogeneities would not match and, consequently, would hinder the distortion correction. To overcome this limitation, subjects could be coached to maintain a somewhat constant respiratory pattern, acquire $b=50 \text{ s/mm}^2$ images with opposite phase encoding interleaved throughout the entire acquisition or automatically detect when drift occurs and discard the affected images before applying distortion correction.

Conclusion

We introduced a novel framework to estimate the respiratory phases of raw DW images using non-linear multi-dimensionality reduction manifold (Laplacian Eigenmaps) to facilitate DisCo and MoCo of free-breathing cardiac DTI. Laplacian Eigenmap-based DisCo and MoCo significantly reduced the geometric distortion and misalignment of the

LV by 13.2%. These improvements are promising, although further work is required to provide reliable distortion correction of single-shot EPI data in cardiac DTI. Ultimately, improvements in geometric distortion of in vivo cardiac DTI with EPI acquisition may enable the potential to improve co-localization of cardiac DTI with alternative contrast MR techniques and potentially facilitate the development of new clinical applications of cardiac DTI. Moreover, distortion-free cardiac DTI acquisition could be used to enable patient-specific electromechanical models of the heart. In this scenario, cardiac DTI would provide microstructure orientation tailored to each patient to inform the preferred direction for electrical propagation in the myocardium as well as the orientation of contraction of the myocytes. The development of these “virtual heart” models would allow applications such as pre-procedure planning(52) and the assessment of personalized risk-stratification(53).

Acknowledgements:

This work was funded by the National Institutes of Health grant numbers R01 HL35242, R01 HL151704, R01 HL141563, and R01 HL131635. Additional support from the Hassenfeld Scholar Award and MGH Corrigan SPARK Award.

REFERENCES:

1. Mekkaoui C, Reese TG, Jackowski MP, Bhat H, Sosnovik DE: Diffusion MRI in the heart. *NMR Biomed* 2017; 30:e3426.
2. Mekkaoui C, Jackowski MP, Kostis WJ, et al.: Myocardial Scar Delineation Using Diffusion Tensor Magnetic Resonance Tractography. *J Am Heart Assoc* 2018; 7:1–10.
3. Ferreira PF, Kilner PJ, McGill L, et al.: In vivo cardiovascular magnetic resonance diffusion tensor imaging shows evidence of abnormal myocardial laminar orientations and mobility in hypertrophic cardiomyopathy. *J Cardiovasc Magn Reson* 2014; 16:1–16.
4. Nielles-Vallespin S, Khalique Z, Ferreira PF, et al.: Assessment of Myocardial Microstructural Dynamics by In Vivo Diffusion Tensor Cardiac Magnetic Resonance. *J*

Am Coll Cardiol 2017; 69:661–676.

5. von Deuster C, Sammut E, Asner L, et al.: Studying Dynamic Myofiber Aggregate Reorientation in Dilated Cardiomyopathy Using In Vivo Magnetic Resonance Diffusion Tensor Imaging. *Circ Cardiovasc Imaging* 2016; 9:1–10.

6. Nguyen CT, Fan Z, Xie Y, et al.: In vivo diffusion-tensor MRI of the human heart on a 3 tesla clinical scanner: An optimized second order (M2) motion compensated diffusion-preparation approach. *Magn Reson Med* 2016; 76:1354–1363.

7. Stoeck CT, von Deuster C, Genet M, Atkinson D, Kozerke S: Second-order motion-compensated spin echo diffusion tensor imaging of the human heart. *Magn Reson Med* 2016; 75:1669–1676.

8. Welsh CL, DiBella EVR, Hsu EW, Di Bella EVR, Hsu EW: Higher-Order Motion-Compensation for in Vivo Cardiac Diffusion Tensor Imaging in Rats. *IEEE Trans Med Imaging* 2015; 34:1843–1853.

9. Aliotta E, Wu HH, Ennis DB: Convex optimized diffusion encoding (CODE) gradient waveforms for minimum echo time and bulk motion-compensated diffusion-weighted MRI. *Magn Reson Med* 2017; 77:717–729.

10. Nguyen CT, Fan Z, Sharif B, et al.: In vivo three-dimensional high resolution cardiac diffusion-weighted MRI: A motion compensated diffusion-prepared balanced steady-state free precession approach. *Magn Reson Med* 2014; 72:1257–1267.

11. Nguyen CT, Christodoulou AG, Coll-Font J, et al.: Free-breathing diffusion tensor MRI of the whole left ventricle using second-order motion compensation and multitasking respiratory motion correction. *Magn Reson Med* 2020:mrm.28611.

12. Riffel P, Michaely HJ, Morelli JN, et al.: Zoomed EPI-DWI of the Pancreas Using Two-Dimensional Spatially-Selective Radiofrequency Excitation Pulses. *PLoS One* 2014; 9:e89468.

13. Reeder SB, Faranesh AZ, Boxerman JL, McVeigh ER: In vivo measurement of T^*2 and field inhomogeneity maps in the human heart at 1.5 T. *Magn Reson Med* 1998; 39:988–998.

14. Meloni A, Hezel F, Positano V, et al.: Detailing magnetic field strength dependence and segmental artifact distribution of myocardial effective transverse relaxation rate at 1.5, 3.0, and 7.0 T. *Magn Reson Med* 2014; 71:2224–2230.

15. Belkin M, Niyogi P: Laplacian Eigenmaps for Dimensionality Reduction and Data Representation. *Neural Comput* 2003; 15:1373–1396.
16. Usman M, Atkinson D, Kolbitsch C, Schaeffter T, Prieto C: Manifold learning based ECG-free free-breathing cardiac CINE MRI. *J Magn Reson Imaging* 2015; 41:1521–1527.
17. Good WW, Erem B, Zenger B, Coll-Font J, Brooks DH, MacLeod RS: Temporal Performance of Laplacian Eigenmaps and 3D Conduction Velocity in Detecting Ischemic Stress. *J Electrocardiol* 2018; 51:S116–S120.
18. Wells lii WM, Viola P, Atsumi H, Nakajima S, Kikinis R: *Multi-Modal Volume Registration by Maximization of Mutual Information. Volume 1*; 1996.
19. Andersson JLR: Geometric Distortions in Diffusion MRI. In *Diffus MRI From Quant Meas to vivo Neuroanat*. Second. Elsevier; 2014:63–85.
20. Chang H, Fitzpatrick JM: A Technique for Accurate Magnetic Resonance Imaging in the Presence of Field Inhomogeneities. *IEEE Trans Med Imaging* 1992; 11:319–329.
21. Jezzard P, Barnett AS, Pierpaoli C: Characterization of and correction for eddy current artifacts in echo planar diffusion imaging. *Magn Reson Med* 1998; 39:801–812.
22. Andersson JLR, Skare S, Ashburner J: How to correct susceptibility distortions in spin-echo echo-planar images: Application to diffusion tensor imaging. *Neuroimage* 2003; 20:870–888.
23. Hedouin R, Commowick O, Bannier E, et al.: Block-Matching Distortion Correction of Echo-Planar Images with Opposite Phase Encoding Directions. *IEEE Trans Med Imaging* 2017; 36:1106–1115.
24. Irfanoglu MO, Modi P, Nayak A, Hutchinson EB, Sarlls J, Pierpaoli C: DR-BUDDI (Diffeomorphic Registration for Blip-Up blip-Down Diffusion Imaging) method for correcting echo planar imaging distortions. *Neuroimage* 2015; 106:284–299.
25. Andersson JLR, Graham MS, Drobniak I, Zhang H, Campbell J: Susceptibility-induced distortion that varies due to motion: Correction in diffusion MR without acquiring additional data. *Neuroimage* 2018; 171:277–295.
26. Verma T, Cohen-Adad J: Effect of respiration on the B0 field in the human spinal cord at 3T. *Magn Reson Med* 2014; 72:1629–1636.
27. Klein S, Staring M, Murphy K, Viergever MA, Pluim J: elastix: A Toolbox for

- Intensity-Based Medical Image Registration. *IEEE Trans Med Imaging* 2010; 29:196–205.
28. Garyfallidis E, Brett M, Amirbekian B, et al.: Dipy, a library for the analysis of diffusion MRI data. *Front Neuroinform* 2014; 8:8.
 29. Lowekamp BC, Chen DT, Ibáñez L, Blezek D: The design of simpleITK. *Front Neuroinform* 2013; 7(DEC).
 30. McCormick M, Liu X, Jomier J, Marion C, Ibanez L: ITK: enabling reproducible research and open science. *Front Neuroinform* 2014; 8(FEB):13–24.
 31. CIBC: Seg3D: Volumetric Image Segmentation and Visualization. Scientific Computing and Imaging Institute (SCI), Download from: <http://www.seg3d.org>. 2016.
 32. Virtanen P, Gommers R, Oliphant TE, et al.: SciPy 1.0: fundamental algorithms for scientific computing in Python. *Nat Methods* 2020; 17:261–272.
 33. Wilcoxon F: Individual Comparisons by Ranking Methods. *Biometrics Bull* 1945; 1:80.
 34. Afacan O, Hoge WS, Wallace TE, Gholipour A, Kurugol S, Warfield SK: Simultaneous motion and distortion correction using dual-echo diffusion weighted MRI. *J Neuroimaging* 2020; 30:276–285.
 35. Gallichan D, Andersson JLR, Jenkinson M, Robson MD, Miller KL: Reducing distortions in diffusion-weighted echo planar imaging with a dual-echo blip-reversed sequence. *Magn Reson Med* 2010; 64:382–390.
 36. Coll-Font J, Afacan O, Hoge WS, et al.: Simultaneous distortion and motion correction in abdominal DW-MRI using dual echo EPI and slice-to-volume. In *Int Soc Magn Reson Med*; 2020.
 37. Schilling KG, Blaber J, Hansen C, et al.: Distortion correction of diffusion weighted MRI without reverse phase-encoding scans or field-maps. *PLoS One* 2020; 15:e0236418.
 38. Graham MS, Drobnyak I, Jenkinson M, Zhang H: Quantitative assessment of the susceptibility artefact and its interaction with motion in diffusion MRI. *PLoS One* 2017; 12:e0185647.
 39. Tunnicliffe E, Andersson JLR, Hess A, Robson M: Feasibility of EPI for cardiac diffusion at 7T. In *Int Soc Magn Reson Med*. Paris, France; 2018.

40. van Gorkum RJH, von Deuster C, Guenthner C, et al.: Analysis and correction of off-resonance artifacts in echo-planar cardiac diffusion tensor imaging. *Magn Reson Med* 2020; 84:mrm.28318.
41. Moulin K, Croisille P, Feiweier T, et al.: In vivo free-breathing DTI and IVIM of the whole human heart using a real-time slice-followed SE-EPI navigator-based sequence: A reproducibility study in healthy volunteers. *Magn Reson Med* 2016; 76:70–82.
42. Chen X, Usman M, Baumgartner CF, et al.: High-Resolution Self-Gated Dynamic Abdominal MRI Using Manifold Alignment. *IEEE Trans Med Imaging* 2017; 36:960–971.
43. Clough JR, Balfour DR, Cruz G, et al.: Weighted Manifold Alignment using Wave Kernel Signatures for Aligning Medical Image Datasets. *IEEE Trans Pattern Anal Mach Intell* 2020; 42:988–997.
44. Earls JP, Ho VB, Foo TK, Castillo E, Flamm SD: Cardiac MRI: Recent progress and continued challenges. *J Magn Reson Imaging* 2002; 16:111–127.
45. Danias PG, McConnell M V., Khasgiwala VC, Chuang ML, Edelman RR, Manning WJ: Prospective navigator correction of image position for coronary MR angiography. *Radiology* 1997; 203:733–736.
46. Huizinga W, Poot DHJ, Guyader J-M, et al.: PCA-based groupwise image registration for quantitative MRI. *Med Image Anal* 2016; 29:65–78.
47. Hodneland E, Hanson EA, Lundervold A, Modersitzki J, Eikefjord E, Munthe-Kaas AZ: Segmentation-driven image registration-application to 4D DCE-MRI recordings of the moving kidneys. *IEEE Trans Image Process* 2014; 23:2392–2404.
48. Marami B, Mohseni Salehi SS, Afacan O, et al.: Temporal slice registration and robust diffusion-tensor reconstruction for improved fetal brain structural connectivity analysis. *Neuroimage* 2017; 156:475–488.
49. Geng X, Ross TJ, Gu H, et al.: Diffeomorphic image registration of diffusion MRI using spherical harmonics. *IEEE Trans Med Imaging* 2011; 30:747–758.
50. Coll-Font J, Afacan O, Chow JS, Lee RS, Warfield SK, Kurugol S: Modeling Dynamic Radial Contrast Enhanced MRI with Linear Time Invariant Systems for Motion Correction in Quantitative Assessment of Kidney Function. *Med Image Anal* 2020; 67:1–12.
51. Taylor AM, Jhooti P, Wiesmann F, Keegan J, Firmin DN, Pennell DJ: MR navigator-

echo monitoring of temporal changes in diaphragm position: Implications for MR coronary angiography. *J Magn Reson Imaging* 1997; 7:629–636.

52. Prakosa A, Arevalo HJ, Deng D, et al.: Personalized virtual-heart technology for guiding the ablation of infarct-related ventricular tachycardia. *Nat Biomed Eng* 2018; 2:732–740.

53. Arevalo HJ, Vadakkumpadan F, Guallar E, et al.: Arrhythmia risk stratification of patients after myocardial infarction using personalized heart models. *Nat Commun* 2016; 7:11437.

FIGURES:

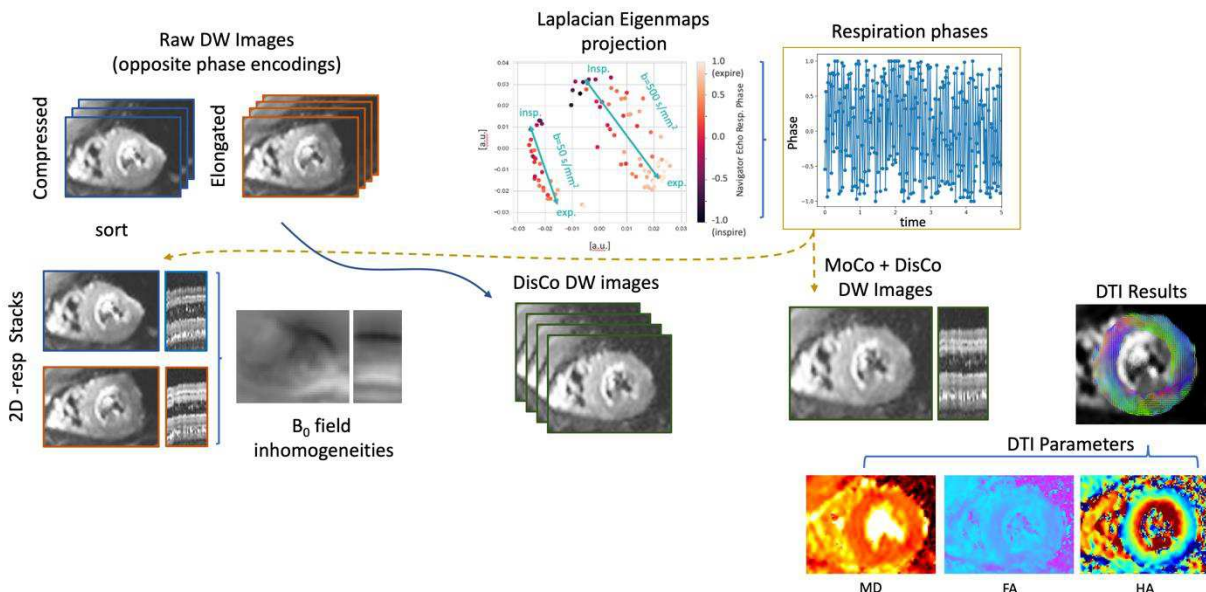


Figure 1. Flow diagram illustrating the LE-based DisCo processing pipeline. The DW images are first embedded into a 2D space with LE to determine their respiratory phase. Afterwards, the images are grouped in stacks of 2D sorted over respiratory phase (2D-resp), which are used to estimate the B_0 field inhomogeneities and correct for distortion.

The images are then binned according to their respiratory phases and the bin centroids are registered to the end-expiration phase. The rest of the images are motion compensated by applying the transformations learned during registration. Finally, the DTI model is fitted to the processed images and its parameters computed.

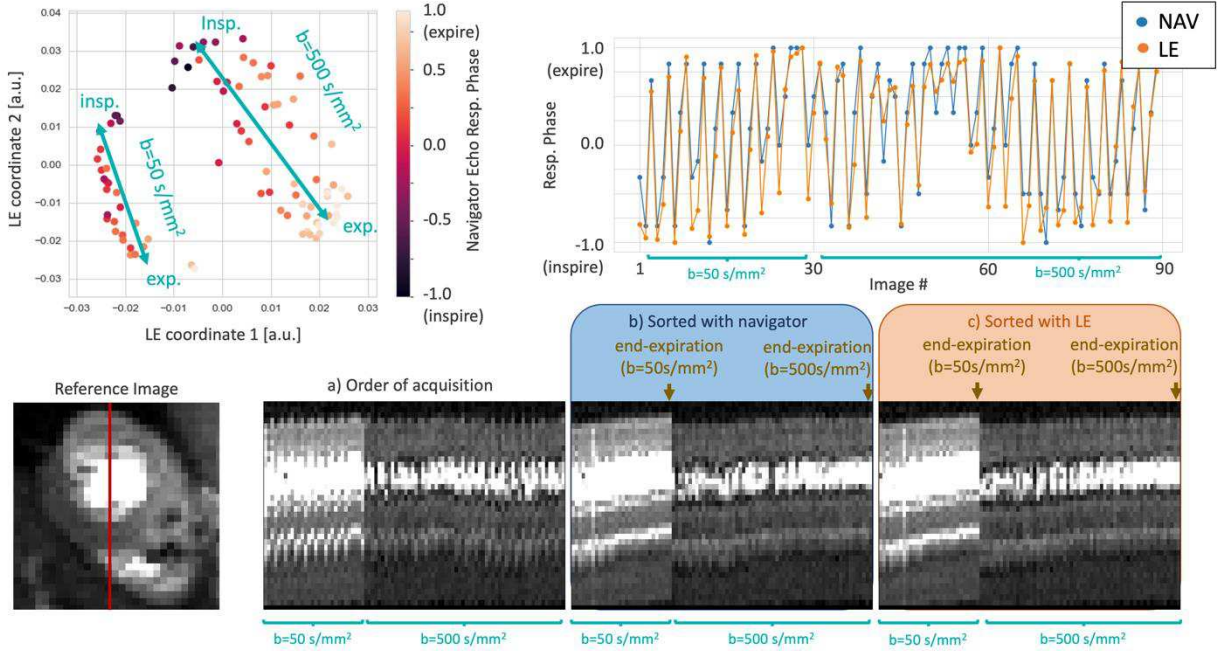


Figure 2. (Top-Left) Example of the low-dimensional representation of the DW images generated with LE. The two clusters of points correspond to different b-values ($b=50$ and 500 s/mm^2) and the elongated direction of the clusters align with the respiratory phases obtained with the navigator echoes, as colormap. (Top-Right) Respiratory phases estimated with the navigator echoes (NAV) and LE in blue and orange, respectively. (Bottom) Line of voxels indicated in the reference image plotted for both b-values sorted over (a) acquisition time, (b) navigator echoes and, (c) LE. The respiratory phases estimated with LE match with those obtained with navigator echoes and both result in similarly sorted DW images.

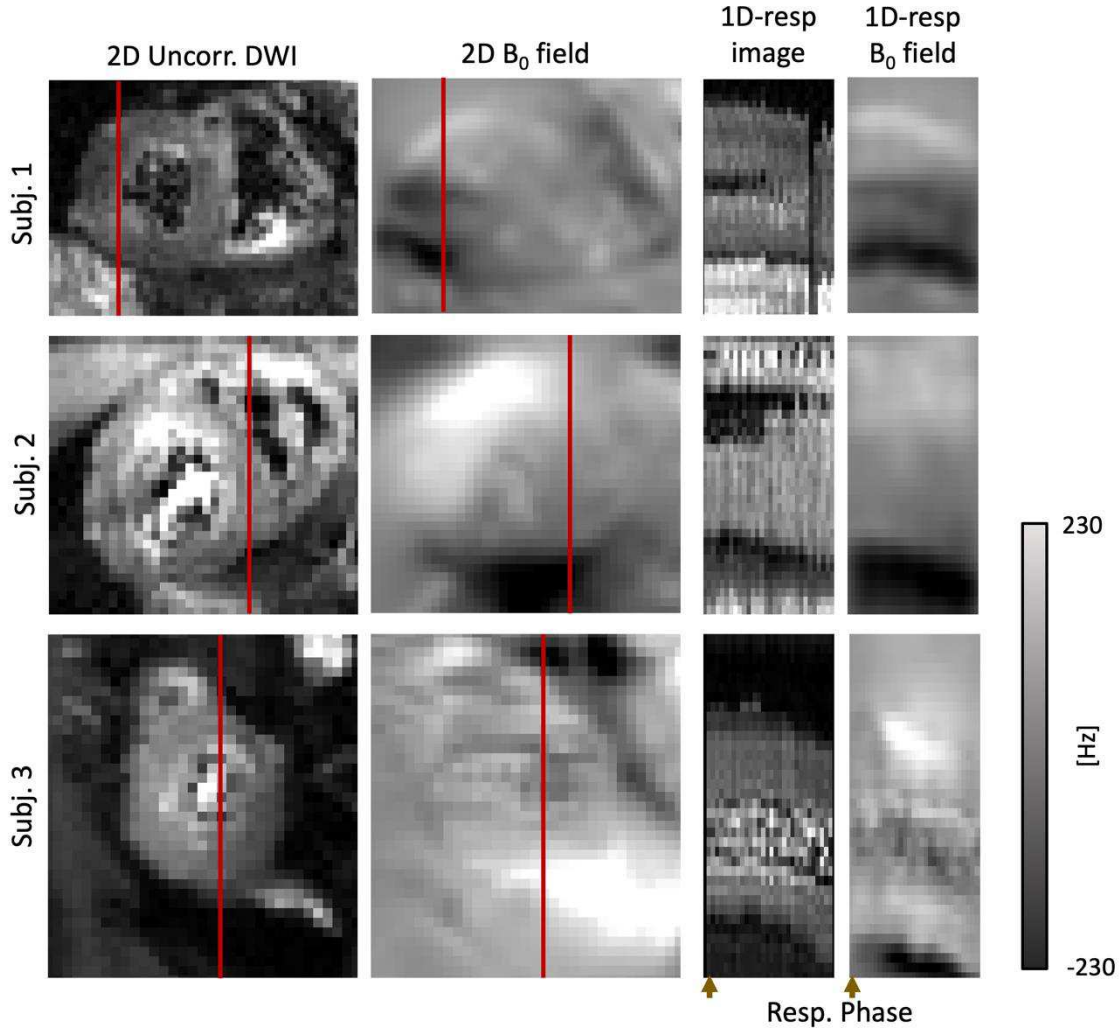


Figure 3. Illustration of the dynamics between distortion and breathing for 3 representative subjects. The first and third columns show 2D DW images and lines of voxels sorted over the respiratory cycle (1D-resp). The red line indicates the line of voxels plotted over time and the yellow arrow the position of the end of expiration in the 2D-resp panels. The second and fourth columns show the 2D and 1D-resp B_0 fields estimated by the DisCo method. The estimated B_0 fields smoothly change over the respiratory cycle.

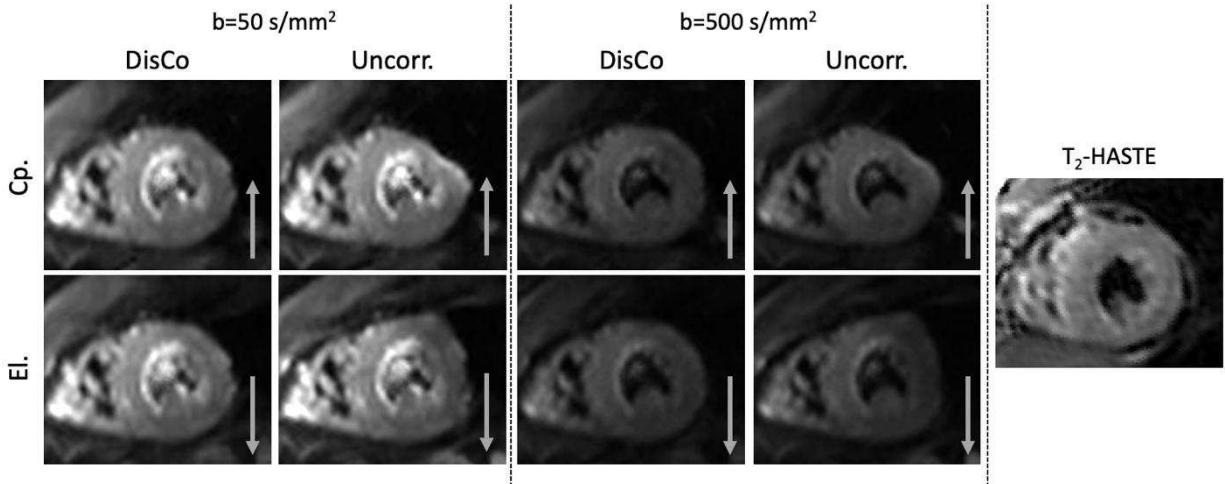


Figure 4. Example DW images compared to their T₂-HASTE reference. The rows correspond to compressed and elongated distortion with phase encode direction indicated by the arrow. The columns show the DisCo and raw images for different b-values. The rightmost image shows the T₂-HASTE reference. DisCo was successful in reducing most of the geometric distortion, resulting in rounder LV geometries, closer to the T₂-HASTE reference.

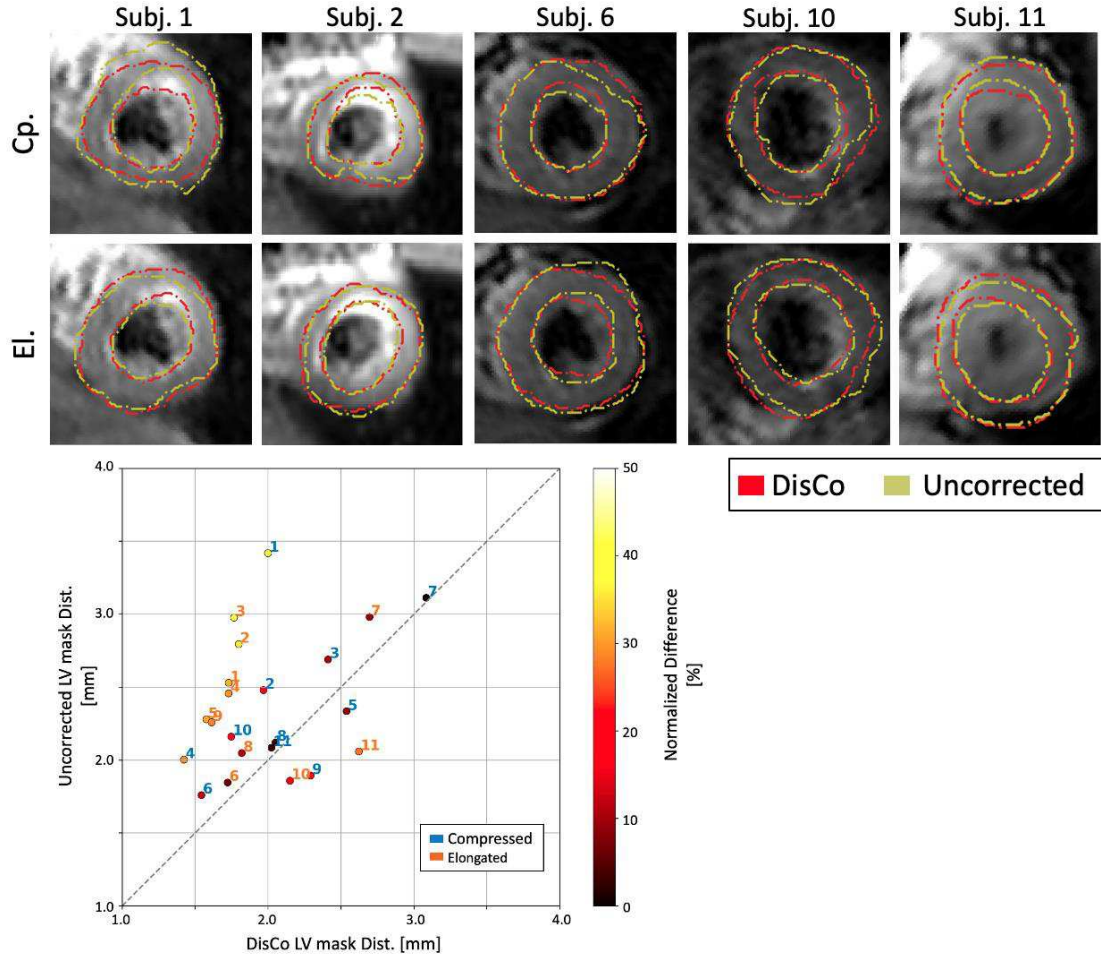


Figure 5. TOP: Contours of LV masks generated with DW images before (yellow) and after (red) overlaid over the corresponding T_2 -HASTE reference. The subjects were sorted according to the distance between their DW and T_2 -HASTE LV masks. The selected subjects correspond to the two subjects with most reduction in distance after applying DisCo, a subject with the median reduction in distance and the two subjects with some increase in error. BOTTOM: Scatter plot of the LV mask distances. Each point corresponds to the LV mask distance obtained with DisCo (horizontal axis) and uncorrected (vertical axis) masks. Most points (18) present a reduction in LV mask distance after DisCo, while 4 present some increase. The colormap highlights the percent absolute difference between DisCo and Uncorrected LV mask distances. The correspondence between the illustrated contours and their position in the scatter plot is indicated with their indices. DisCo succeeded in reducing the distortion for most subjects.

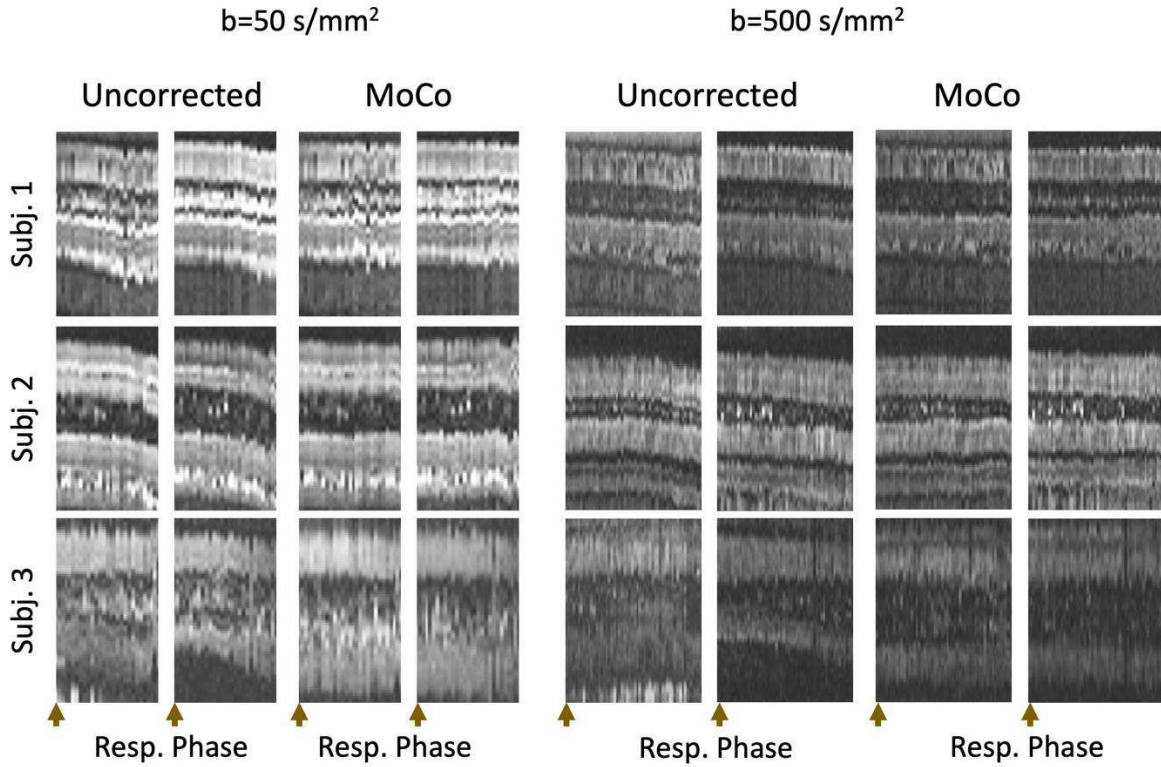


Figure 6. Line of voxels plotted along the respiratory phase (1D-resp) before and after registration. The yellow arrow indicates the end of expiration phase in each panel. Before MoCo, the heart smoothly moves from top to bottom with inspiration. After MoCo the LV is aligned throughout the respiratory cycle.

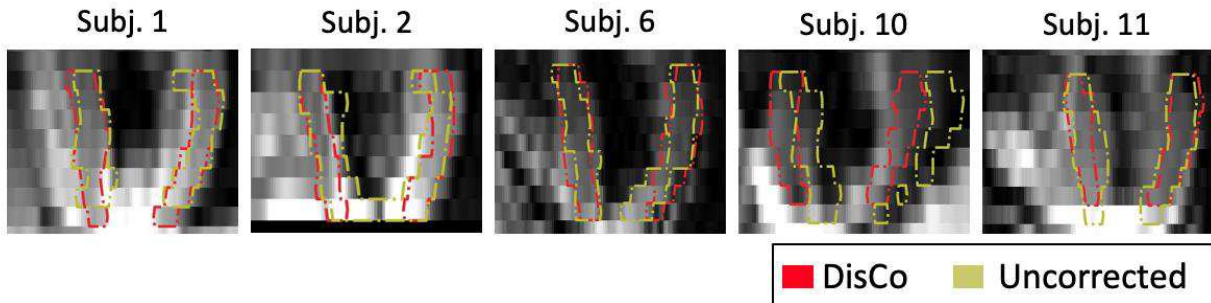


Figure 7. Long axis view of representative DW masks obtained before (yellow) and after (red) MoCo overlaid over the reference T₂-HASTE image acquired during breath-

hold. Registration to the end-expiration phase allowed for through-slice alignment that is consistent with the breath-hold acquisition.

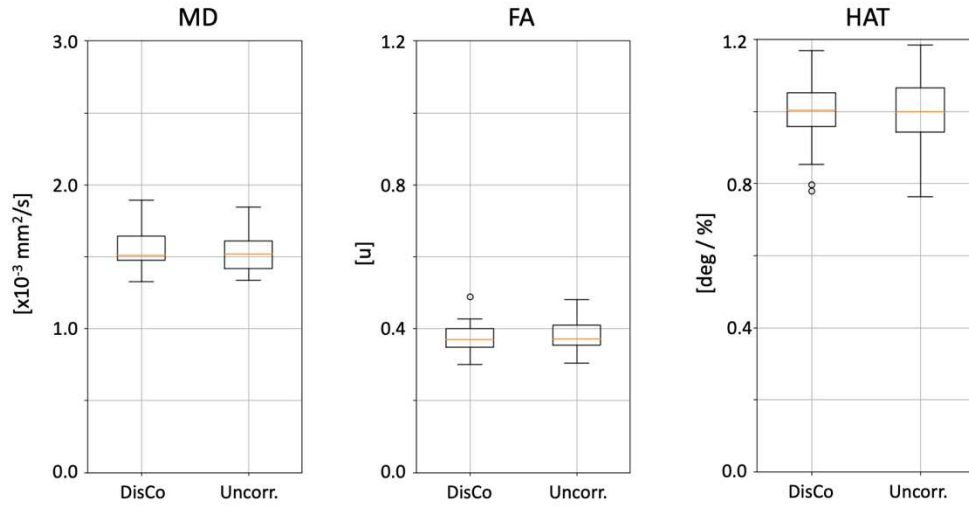


Figure 8. Boxplot with all DTI parameter values (MD, FA and HAT) computed on the uncorrected DW images (only MoCo was applied) and the DisCo images. DisCo did not produce significant changes in MD, FA nor HAT.

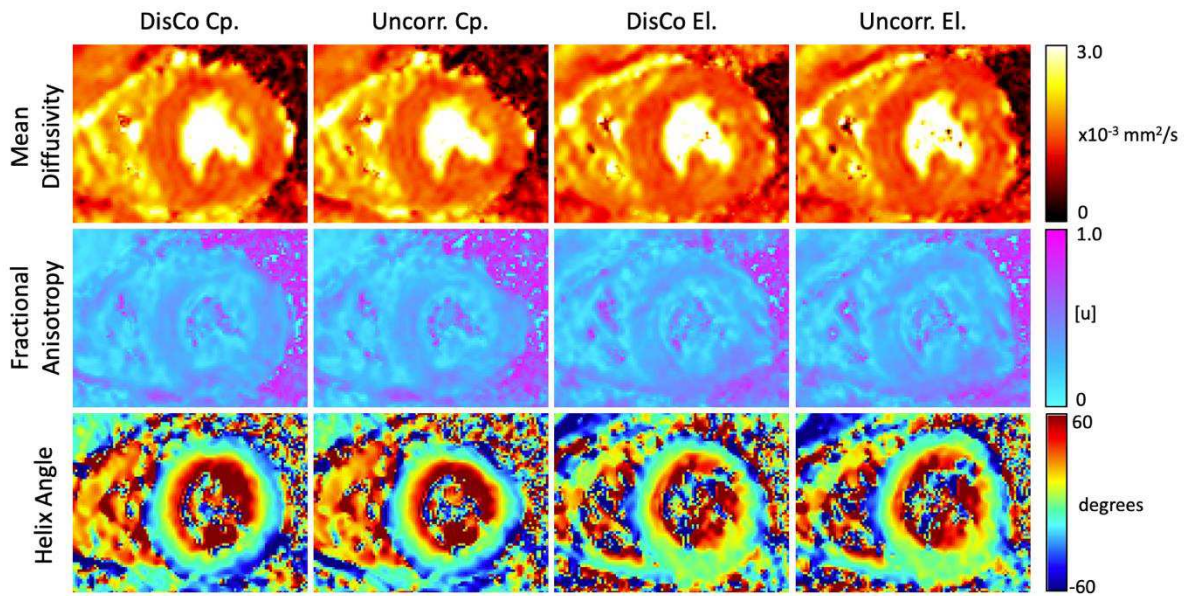


Figure 9. Parameter maps (MD, FA and HA) computed on the DW images with and without applying DisCo. DisCo did not change the values obtained in the parameter maps although the shape of the LV was rounder after performing DisCo. The images acquired along the ‘elongated’ phase encoding resulted in disrupted HA maps in the stretched area.

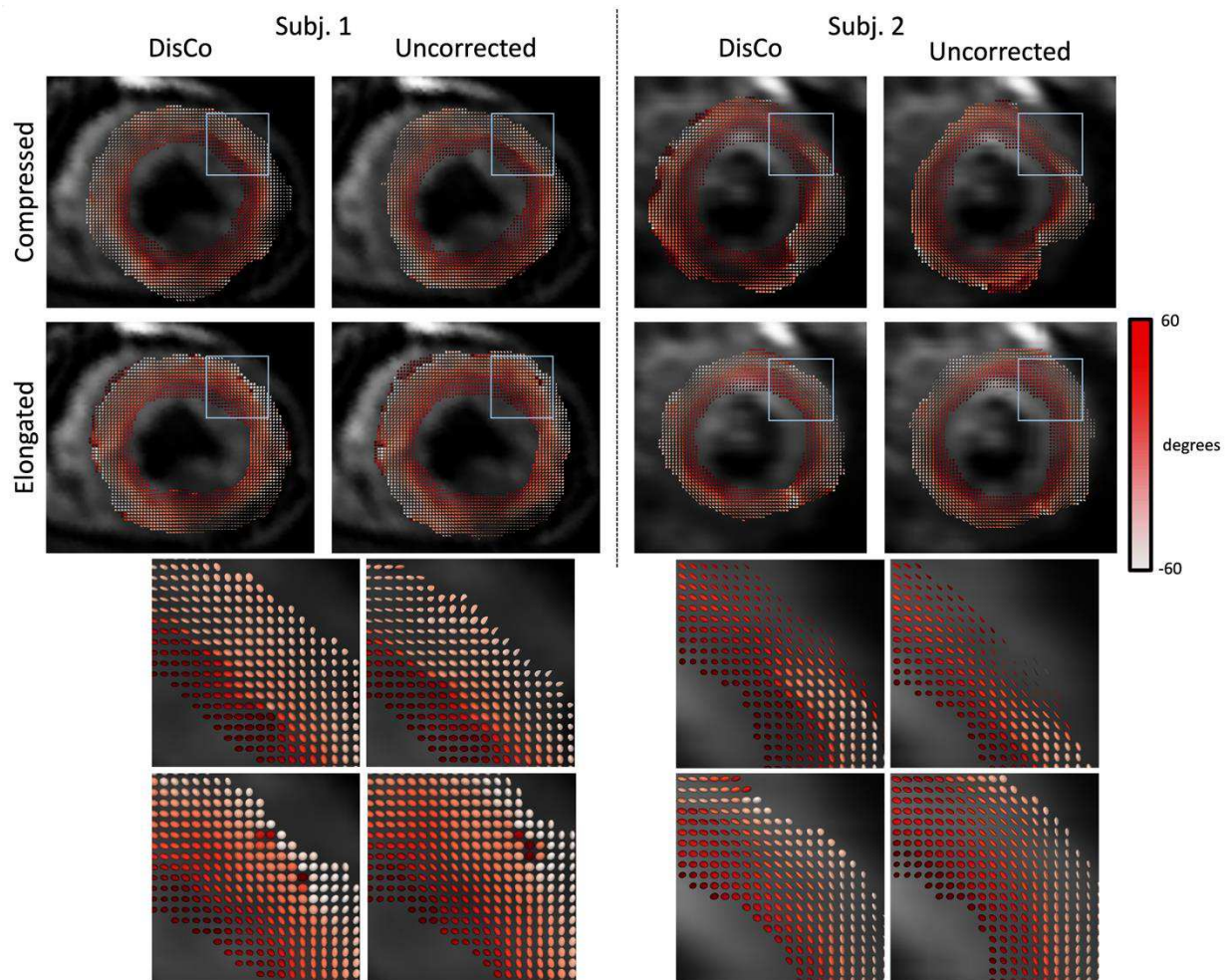
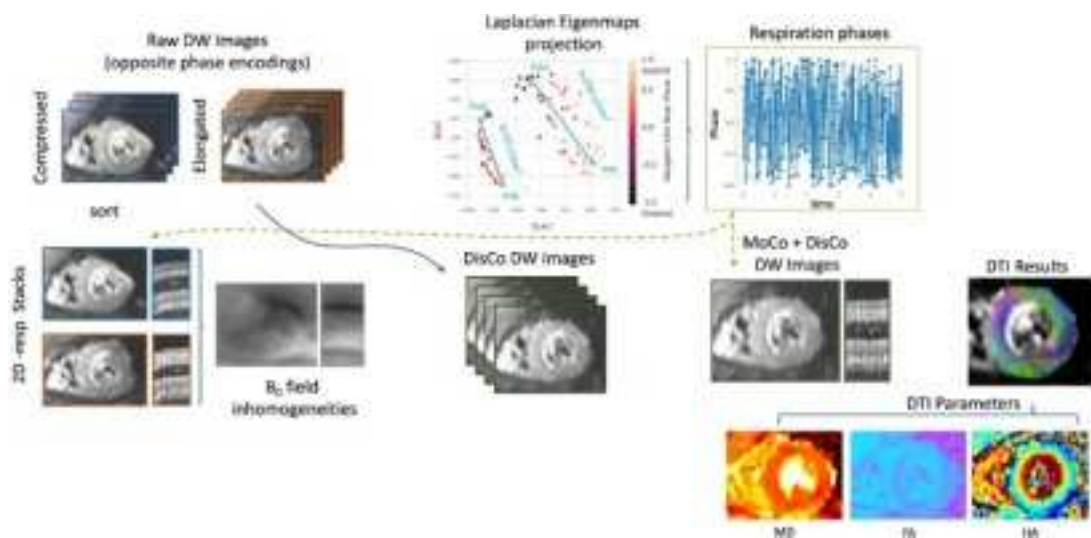
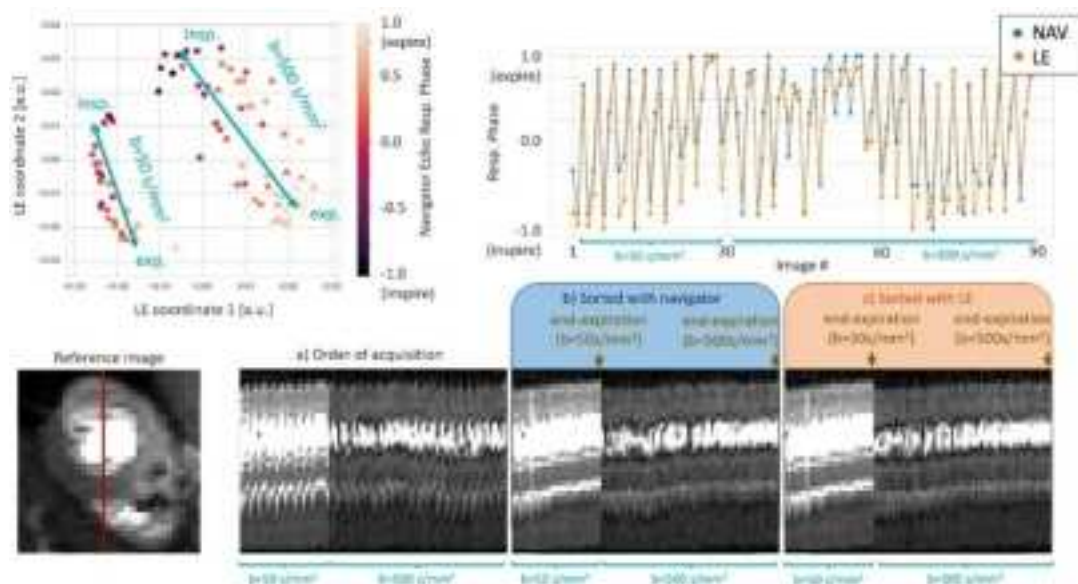


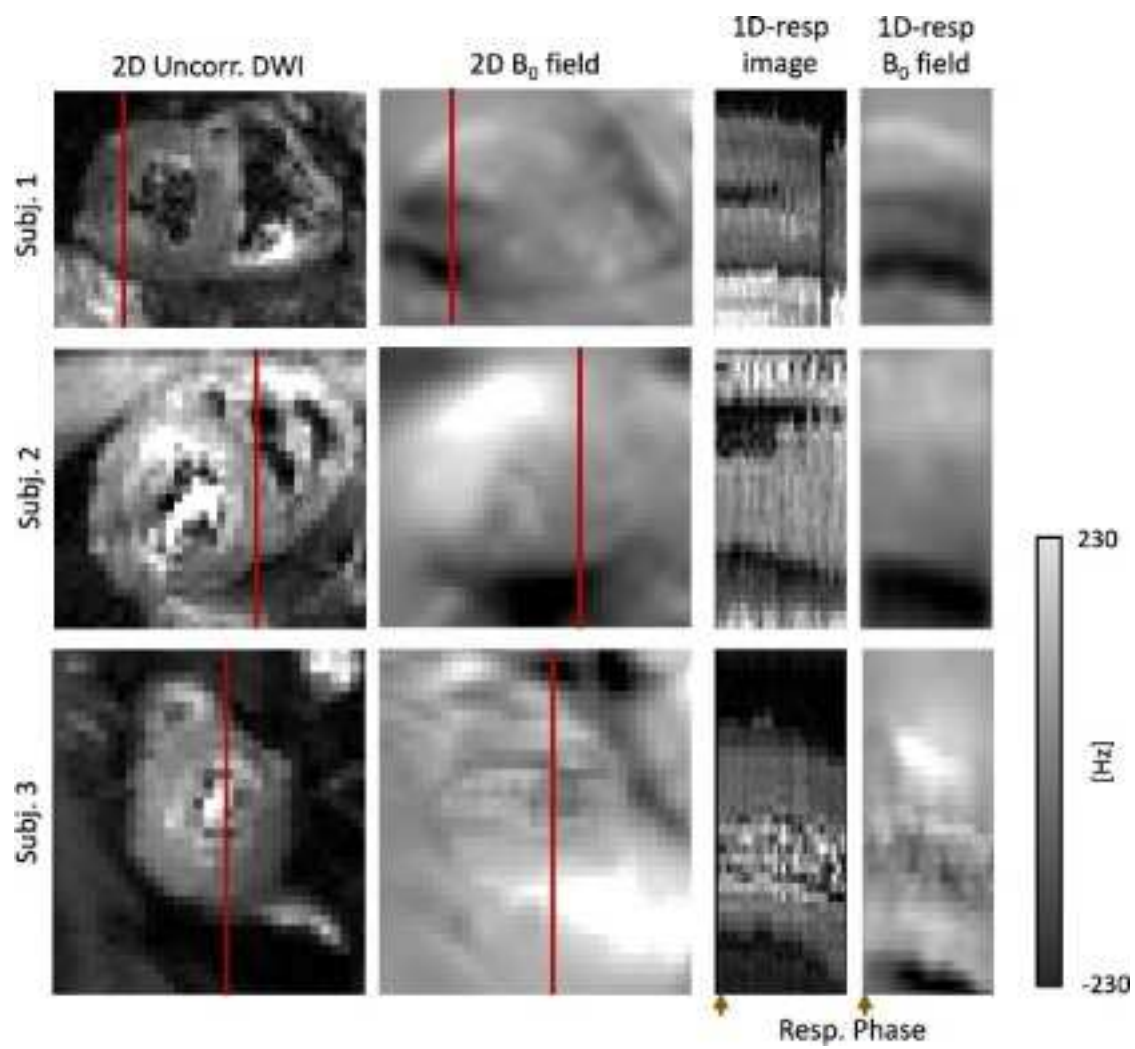
Figure10. Diffusion tensor orientation in two representative subjects obtained with the DW images with and without DisCo and colored according to their helix angle. The areas indicated with a blue square are enlarged below for better visualization. The geometry deformation resulted in displacement of the diffusion tensors and, consequently, affected the direction of the estimated micro-structure.



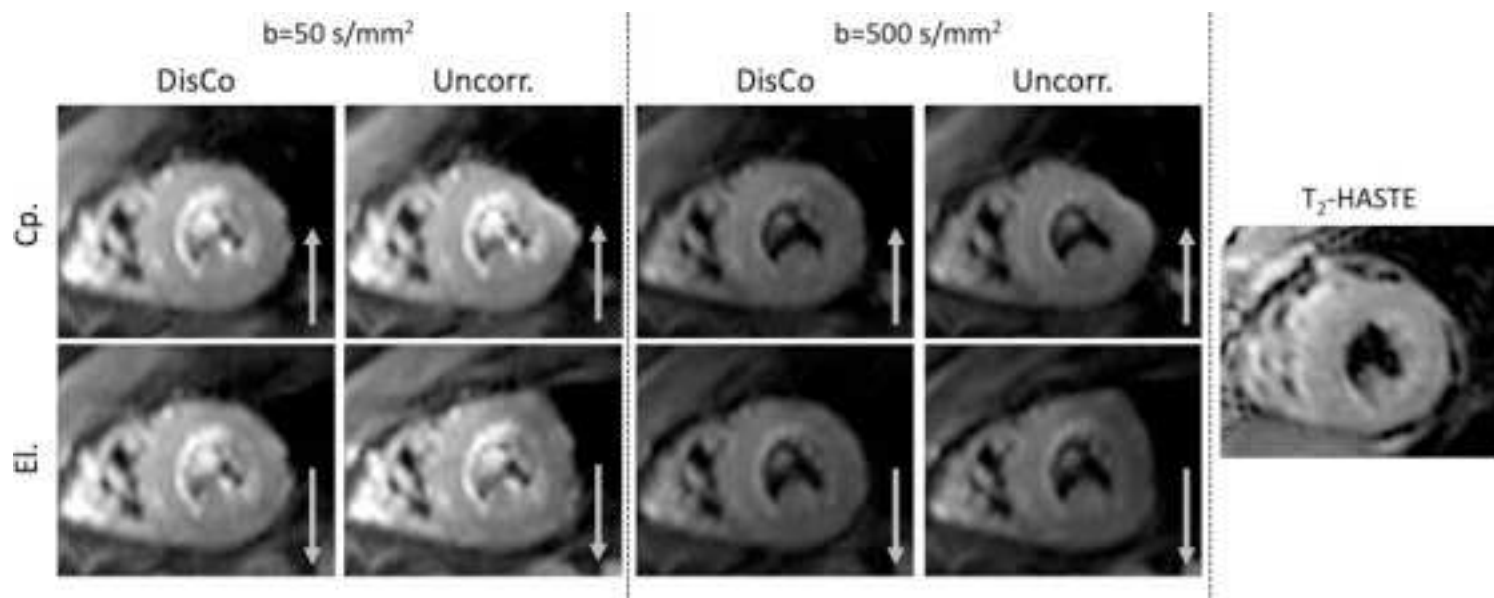
mrm_28972_f1.tiff



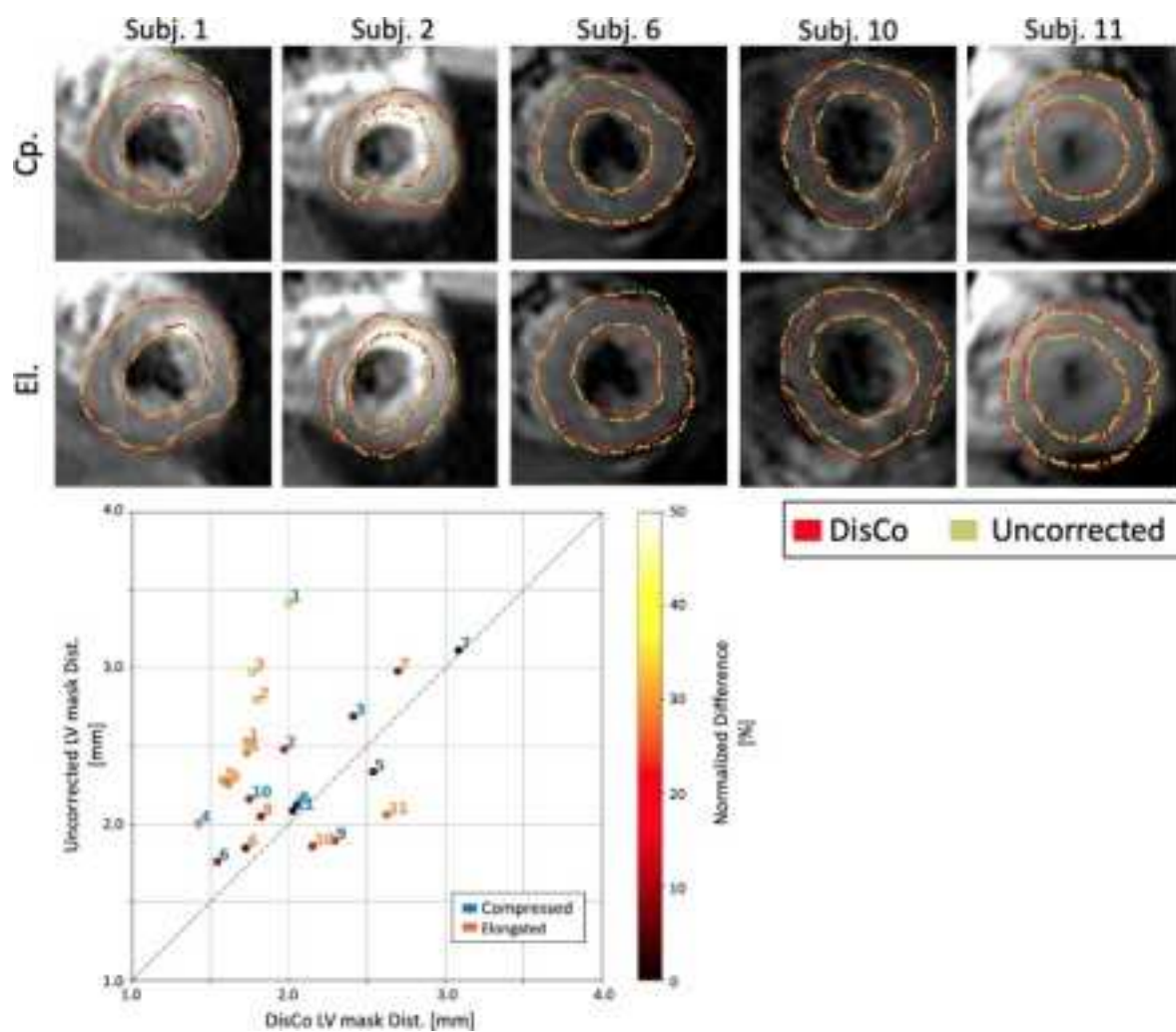
mrm_28972_f2.tiff



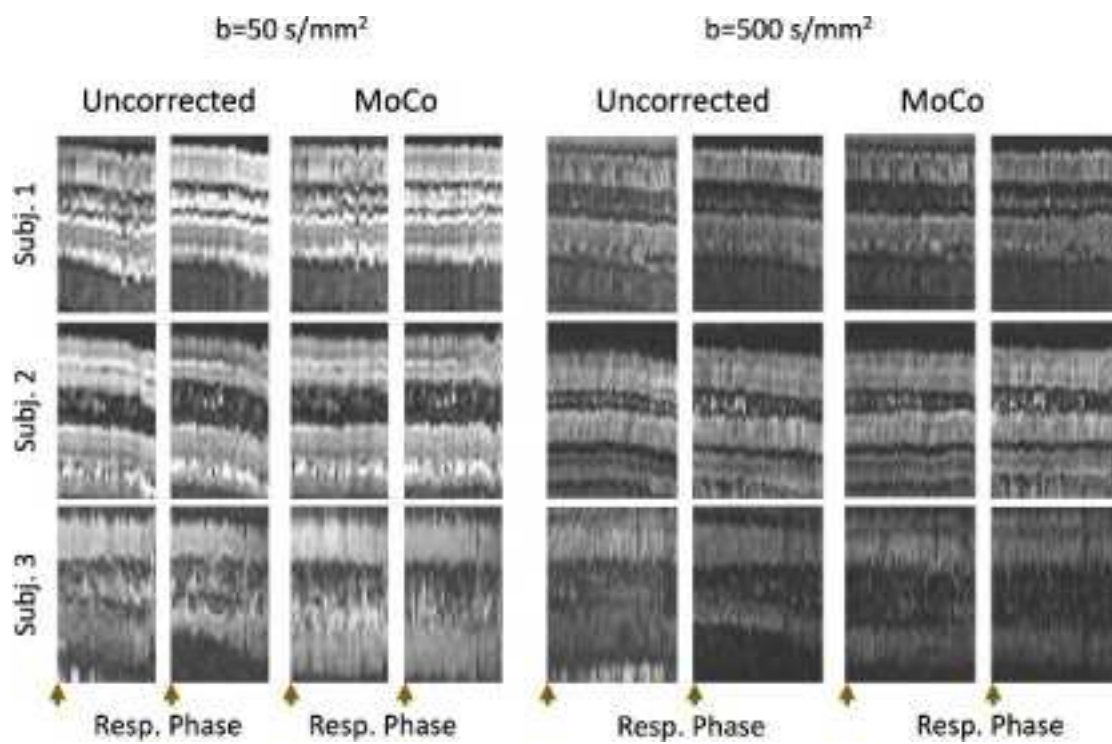
mrm_28972_f3.tiff



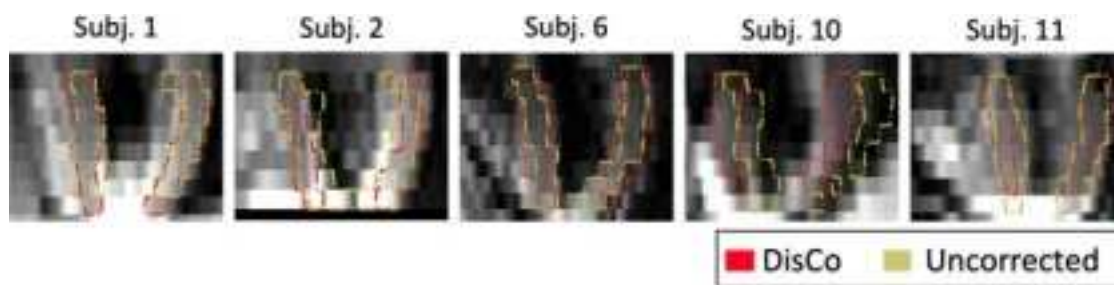
mrm_28972_f4.tiff



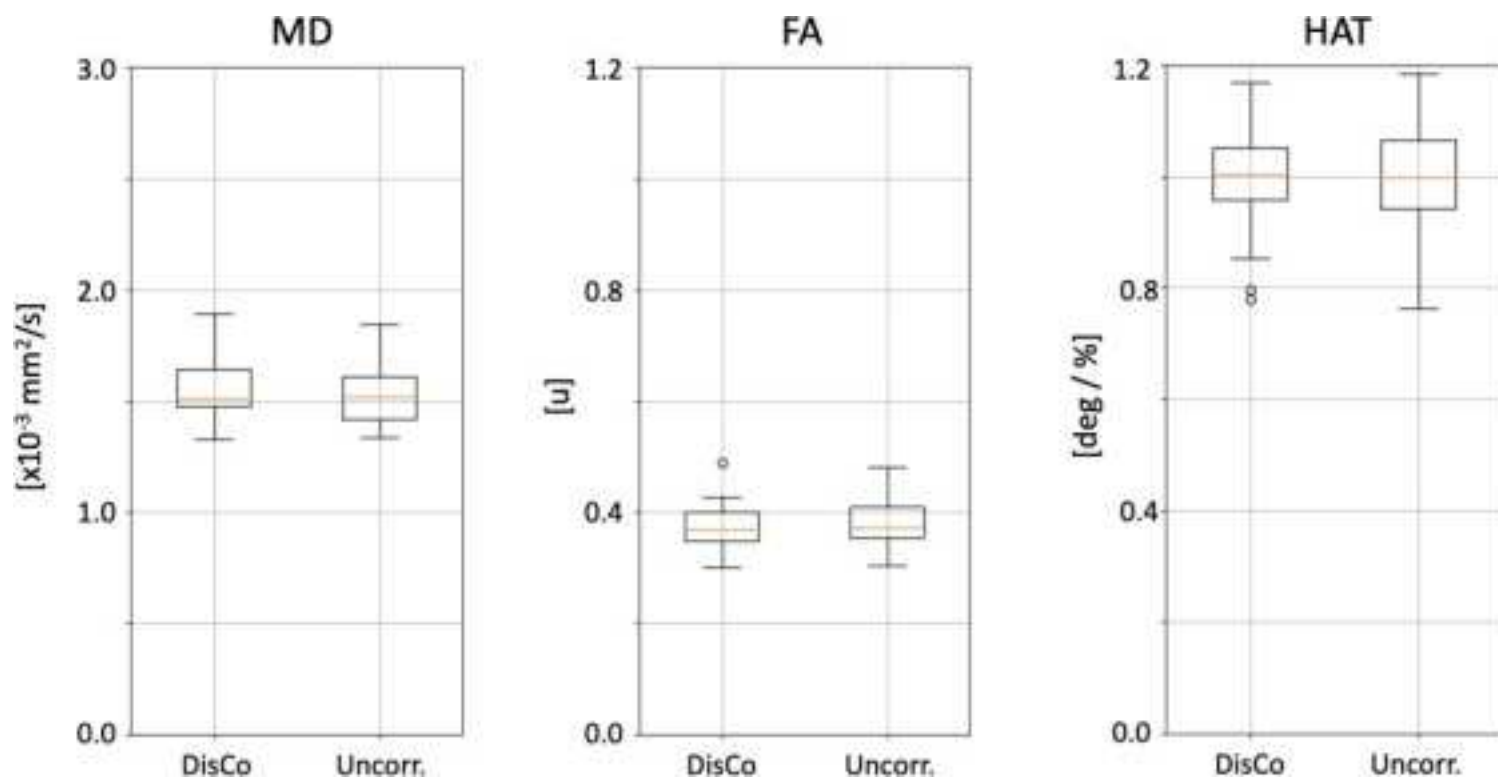
mrm_28972_f5.tiff



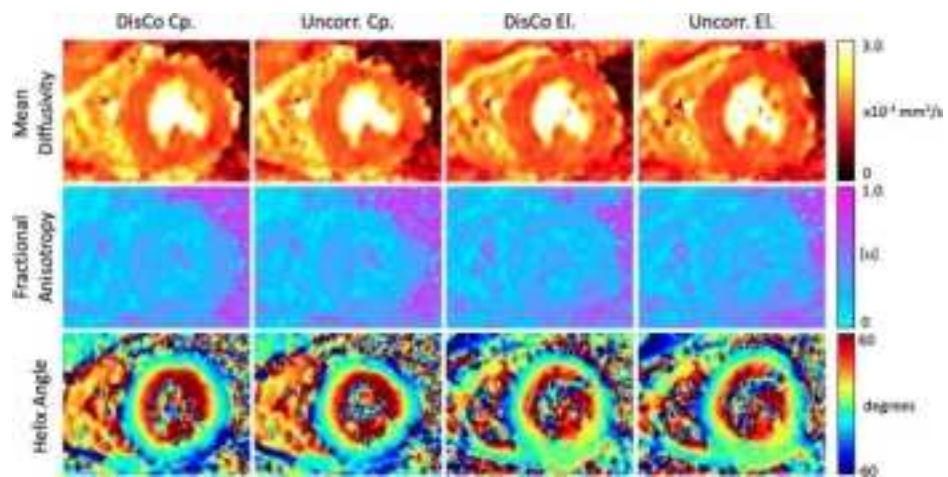
mrm_28972_f6.tiff



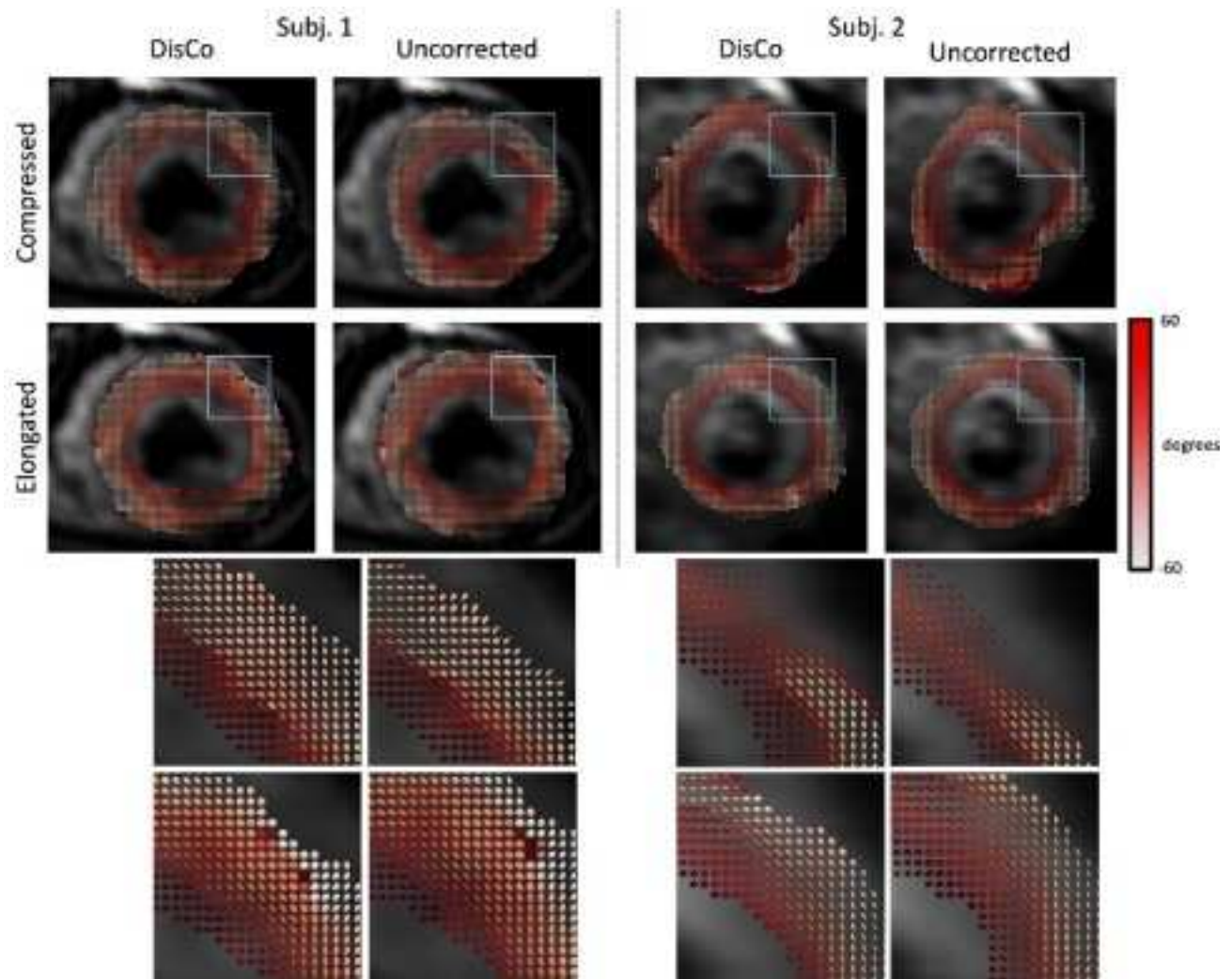
mrm_28972_f7.tiff



mrm_28972_f8.tiff



mrm_28972_f9.tiff



mrm_28972_f10.tiff